Cell

Short article

Human orbitofrontal neural activity is linked to obsessive-compulsive behavioral dynamics

Graphical abstract

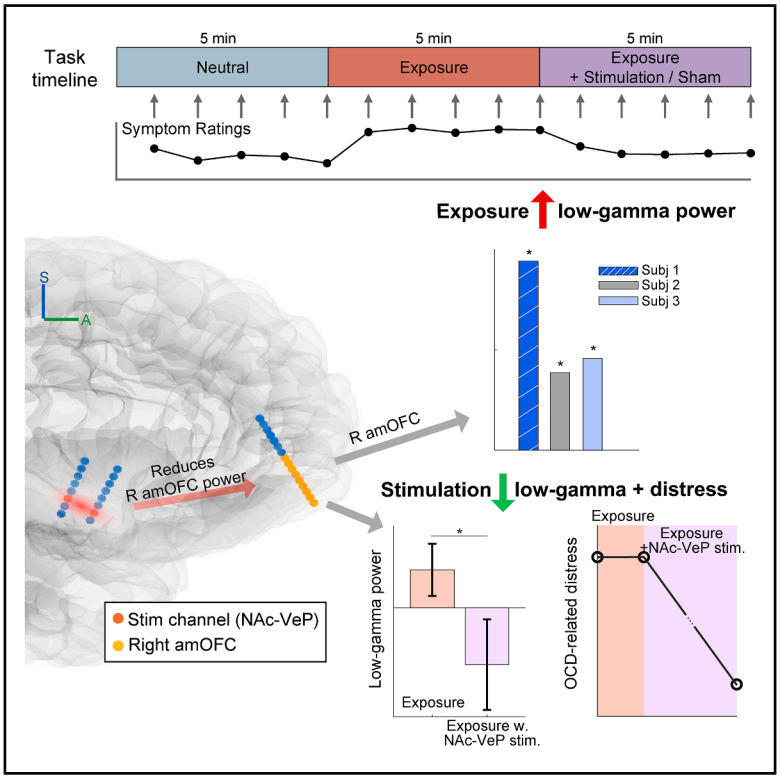

Authors

Young-Hoon Nho, Liming Qiu, Robert L. Seilheimer, ..., Kai J. Miller, Katherine W. Scangos, Casey H. Halpern

Correspondence

katherine.scangos@Pennmedicine.upenn.edu (K.W.S.), casey.halpern@pennmedicine.upenn.edu (C.H.H.)

In brief

Stimulating ventral basal ganglionic targets modulates a dynamic amOFC biomarker linked to OCD, providing insights into network dynamics and supporting the development of personalized, electrophysiology-guided deep brain stimulation for improved neuromodulation treatment.

Highlights

- Right amOFC low-gamma tracks OCD-related distress during provocation
- Ventral basal ganglia stimulation had robust acute reduction in OCD-related distress
- Ventral basal ganglia stimulation reduces amOFC low-gamma and improves OCD symptoms

Nho et al., 2026, Cell *189*, 739–747
February 5, 2026
https://doi.org/10.1016/j.cell.2025.12.037

CellPress

Cell

CellPress
OPEN ACCESS

Short article

Human orbitofrontal neural activity is linked to obsessive-compulsive behavioral dynamics

Young-Hoon Nho,[1,11] Liming Qiu,[1,11] Robert L. Seilheimer,[1,2] Gustavo Campos,[1] Andrew Chang,[1] Zhengjia Wang,[1] John F. Magnotti,[1] Michael S. Beauchamp,[1] Daniel A.N. Barbosa,[1,3] Andreas Horn,[4] Nolan R. Williams,[5,12] Lily A. Brown,[2] Taneeta M. Ganguly,[6] Mario Cristancho,[2] Bijan Pesaran,[1,7,8] Desmond J. Oathes,[2] Kai J. Miller,[9] Katherine W. Scangos,[1,2,*] and Casey H. Halpern[1,10,13,*]

[1]Department of Neurosurgery, Perelman School of Medicine, University of Pennsylvania, Philadelphia, PA, USA
[2]Department of Psychiatry, Perelman School of Medicine, University of Pennsylvania, Philadelphia, PA, USA
[3]Departments of Neurology, Psychiatry and Behavioral Sciences, Medical University of South Carolina, Charleston, SC, USA
[4]Institute for Network Stimulation, Department of Stereotactic and Functional Neurosurgery, University Hospital Cologne, Cologne, Germany
[5]Department of Psychiatry and Behavioral Sciences, Stanford University, Palo Alto, CA, USA
[6]Department of Neurology, Perelman School of Medicine, University of Pennsylvania, Philadelphia, PA, USA
[7]Department of Bioengineering, University of Pennsylvania, Philadelphia, PA, USA
[8]Department of Neuroscience, University of Pennsylvania, Philadelphia, PA, USA
[9]Department of Neurosurgery, Mayo Clinic, Rochester, MN, USA
[10]Department of Surgery, Corporal Michael J. Crescenz Veterans Affairs Medical Center, Philadelphia, PA, USA
[11]These authors contributed equally
[12]Deceased
[13]Lead contact
*Correspondence: katherine.scangos@Pennmedicine.upenn.edu (K.W.S.), casey.halpern@pennmedicine.upenn.edu (C.H.H.)
https://doi.org/10.1016/j.cell.2025.12.037

SUMMARY

Biomarkers of obsessive-compulsive disorder (OCD) symptom dynamics and related behavior could advance personalized interventions. Aberrant activity in the orbitofrontal cortex (OFC) has been implicated in symptom exacerbation in OCD. We conducted an intracranial monitoring assay to identify high-resolution neurophysiologic correlates of OCD symptoms in the human OFC. We found that low-gamma power in the anteromedial OFC was consistently elevated during high symptom states in a symptom provocation task. Furthermore, electrical stimulation of the ventral basal ganglia that reduced OCD symptoms also reduced anteromedial OFC gamma power. These results link OFC gamma activity to moment-to-moment expression of OCD symptoms, providing mechanistic insights to guide therapeutic strategies such as deep brain stimulation.

INTRODUCTION

Obsessive-compulsive disorder (OCD) is a common (2%–3% lifetime prevalence) and disabling psychiatric disorder.[1,2] At least 30% of patients with OCD do not adequately respond to conventional treatment, which includes psychotherapy (e.g., exposure and response prevention), psychotropic medications, and their combination.[3,4] Accumulating and converging multimodal evidence implicates dysregulated fronto-basal ganglia circuitry in the pathophysiology of OCD, including altered activity in the orbitofrontal cortex (OFC) and basal ganglia.[5–7] Therapeutic strategies that modulate this dysfunctional circuit are emerging,[8] including deep brain stimulation (DBS),[9,10] which received humanitarian device exemption approval from the FDA in 2009 for this indication. Reported response rates to DBS for OCD average around 66% in open-label and controlled trials.[11]

However, traditional DBS delivers continuous stimulation without feedback, and it remains unclear how this stimulation engages the underlying neural circuitry or drives clinical responses.[12] Understanding how neural activity maps to symptom expression is critical not only for optimizing target selection but also for developing biomarker-informed, closed-loop DBS systems.[13,14] Such systems could improve clinical outcomes by aligning stimulation delivery with relevant brain states, thereby enhancing efficacy, minimizing side effects, promoting plasticity, and allowing symptom-specific targeting.

Despite its centrality to fronto-basal ganglia circuitry, the OFC remains underexplored in human intracranial studies of OCD. The OFC is thought to be involved in reward valuation, decision-making, and affective and motivational processes—all of which are disrupted in OCD.[15,16] Imaging studies suggest that the OFC shows state-dependent fluctuations in activity that correlate with obsessions and compulsions, yet direct electrophysiological evidence remains limited.[17–20] We hypothesized that neural activity in OFC would reflect OCD symptom-related internal states, particularly distress, and that it would exhibit temporal dynamics suitable for closed-loop neuromodulation.

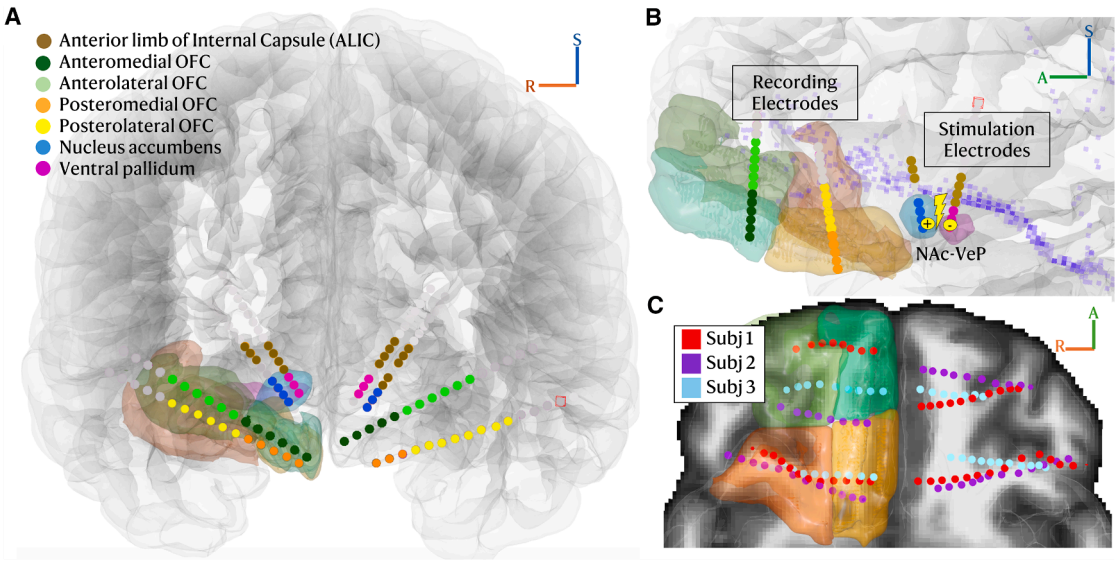

Figure 1. sEEG electrode localization

(A) SEEG electrodes were placed in cortical and subcortical targets implicated in the OCD network in each subject (coronal view). Each region is color-coded according to the legend.

(B) Spatial representation of stimulating electrodes in the nucleus accumbens and ventral pallidum (NAc/VeP), as well as recording electrodes in the orbitofrontal cortices (OFC) (mid-sagittal view, right hemisphere). Fronto-basal ganglia streamlines are overlaid in light purple.

(C) Placement of orbitofrontal sEEG electrodes in all three subjects in a normalized MNI-152 template space (axial view). The right OFC is shown with division into the anteromedial (teal), anterolateral (green), posteromedial (yellow), and posterolateral (orange) regions.

See also Figure S1.

To test this hypothesis, we leveraged a clinical trial involving stereo-electroencephalography (sEEG)-guided DBS for treatment-refractory OCD (NCT05623306; see STAR Methods).[21] In this intracranial monitoring study, we performed recordings with high-temporal resolution from the OFC and subcortical targets during an individualized symptom provocation task, enabling us to examine dynamic neural correlates of OCD symptoms in real time. Electrodes were implanted in cortical and subcortical regions implicated in OCD-related circuitry, and patients underwent intensive inpatient evaluation in the psychiatric monitoring unit of Pennsylvania Hospital (University of Pennsylvania Health System) (Figures 1A–1C).

This approach allowed us to identify candidate electrophysiologic biomarkers of obsessive-compulsive symptom states to explore how such signals might support patient-specific, brain state-dependent targeted neuromodulation interventions. Ultimately, this work aims to advance a new era of precision neuromodulation for neuropsychiatric disorders.

RESULTS

NAc-VeP stimulation produced the most robust acute reduction in OCD-related distress, supporting its potential as a key target for symptom-specific neuromodulation

Three subjects in this study were enrolled in a clinical trial of sEEG-guided DBS for treatment-refractory OCD (NCT05623306). SEEG electrodes were implanted in cortical and subcortical nodes involved in OCD-related networks in order to identify personalized DBS targets and delineate the mechanistic underpinnings of acute and chronic stimulation (Figures 1A–1C).

We first evaluated the acute clinical effects of direct electrical stimulation to targets in the anterior limb of the internal capsule (ALIC) and extended ventral striatal territory to identify the stimulation site with the most robust therapeutic potential. This included the ventral pallidum (VeP) in close proximity to the anterior commissure and other adjacent ventral basal ganglionic structures (see STAR Methods; target evaluation session; Figures 2A and S1). Our target regions included the ALIC, nucleus accumbens (NAc), bed nucleus of the striae terminalis (BNST), and VeP.[22] Given our prior experience with the NAc-VeP complex, we also examined clinical effects when stimulating this complex.[23] Small studies have shown promise for DBS at each of these targets[22–25] but the optimal DBS location at the individual level may vary across patients due to disease heterogeneity. Here, we sought to identify the most promising stimulation site in a sham-controlled fashion with the largest acute effect on OCD symptoms. The goal was to link those symptom-specific changes to biomarker activity—specifically, activity that is amenable to modulation by DBS.

We compared the change in OCD symptoms following acute electrical stimulation of contacts within the ALIC, NAc, VeP, and NAc-VeP (Figure 2A) using a 0–10 visual analog scale (VAS) of OCD distress, a measure of how severely OCD-related symptoms were experienced by the subject in the moment. The acute reduction in OCD distress levels (with blinded, 1- or 5-min stimulation trials conducted over 5 days; see STAR Methods) for each stimulation condition was as follows: 33.3% for NAc-VeP

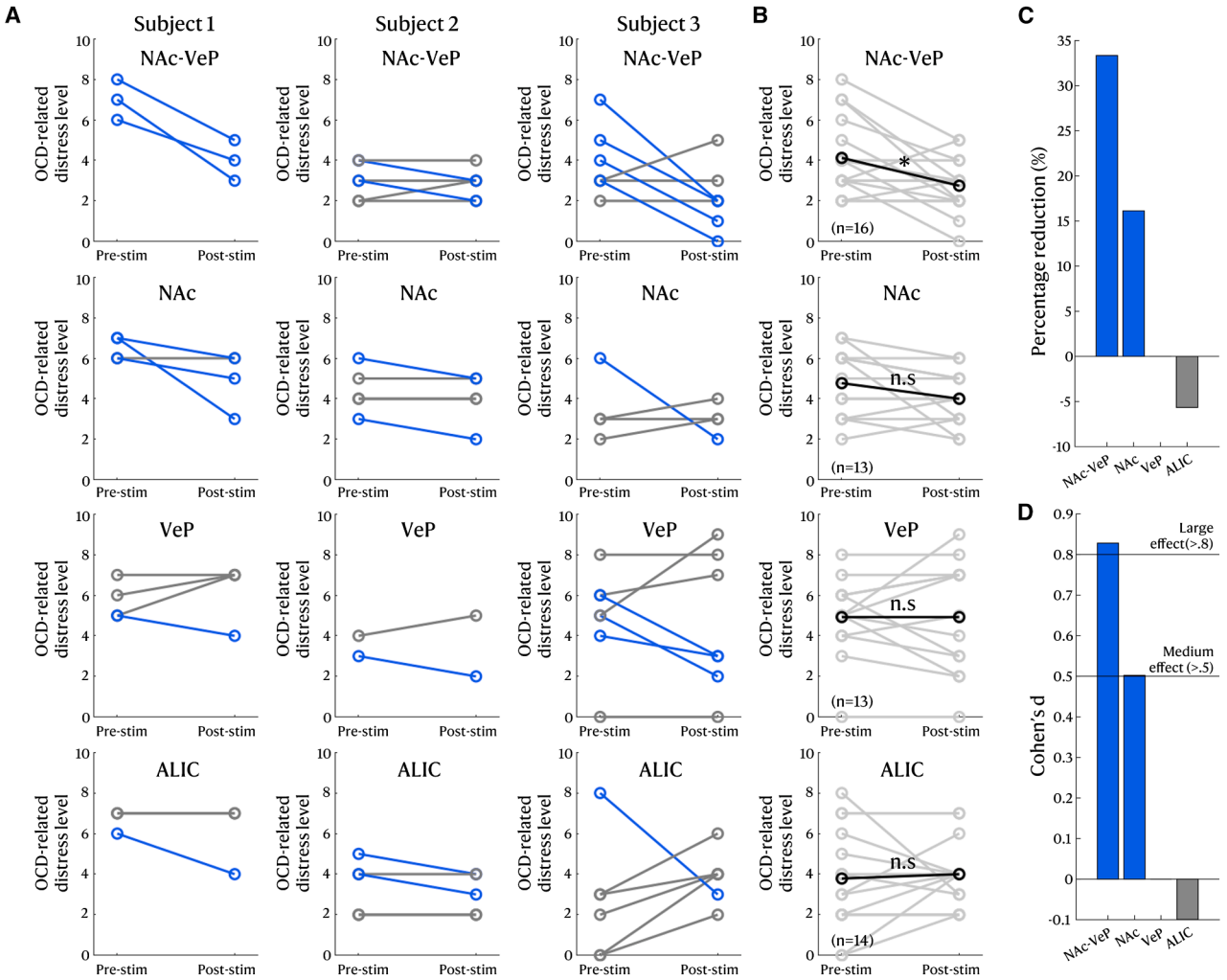

Figure 2. Individual acute effects of NAc-VeP, NAc, VeP, and ALIC stimulation on OCD symptoms during the target evaluation session

(A) Acute effects of NAc-VeP, NAc, VeP, and ALIC stimulation on OCD symptoms during the target evaluation session for each subject. Each row represents symptom changes between pre- and post-stimulation for NAc-VeP (top row), NAc (second row), VeP (third row), and ALIC (bottom row). The connected dot plots illustrate individual symptom changes, with blue representing positive therapeutic outcomes and gray representing no change or negative outcomes.

(B) Average symptom changes across the three subjects demonstrate a significant reduction (*p = 0.013, n = 16) during NAc-VeP stimulation.

(C and D) NAc-VeP stimulation resulted in the largest symptom reduction (33.33%; C) and had the largest effect size (d = 0.83; D), suggesting it was the most effective acute stimulation target compared with other sites.

(d = 0.83, n = 16), 16.2% for NAc (d = 0.50, n = 13), 0.0% for VeP (d = 0.00, n = 13), and −5.7% for ALIC (d = −0.10, n = 14) (Figures 2B–2D; Table S1). Notably, NAc-VeP stimulation led to a significant reduction in distress (*p = 0.013; Figure 2B) and had the largest effect size across the cohort (Figure 2D).

Right amOFC low-gamma activity tracks OCD-related distress state during provocation

We next examined neural activity in the OFC to identify neural correlates of OCD-related distress. Subjects underwent a psychologist-led symptom provocation task using individualized exposure protocols modeled after validated exposure-response prevention (ExRP) therapy.[26] Each subject engaged in 3–11 trials of symptom provocation in which they were exposed to 5 min of a neutral stimulus followed by 5 min of an OCD-provoking stimulus akin to an exposure in ExRP, followed by relaxation to alleviate OCD-related symptoms (Figure 3A).

Exposure to distressing stimuli resulted in significant alterations in low-gamma (30–55 Hz) power across all OFC subregions, with both increases and decreases observed relative to neutral stimuli (Figure 3B). Notably, we observed a consistent elevation in low-gamma frequency band (30–55 Hz) power in the right anteromedial OFC (amOFC) region across all three subjects (*p = 1.22e^{-14}, n_{Neu} = 288, n_{Exp} = 284; *p = 0.014, n_{Neu} = 203, n_{Exp} = 167; *p = 9.69e^{-6}, n_{Neu} = 652, n_{Exp} = 688 in subjects 1, 2, and 3, respectively; Figure 3C). Elevated amOFC low-gamma power was consistently present across different days of symptom provocation tasks and in each subject. In order to

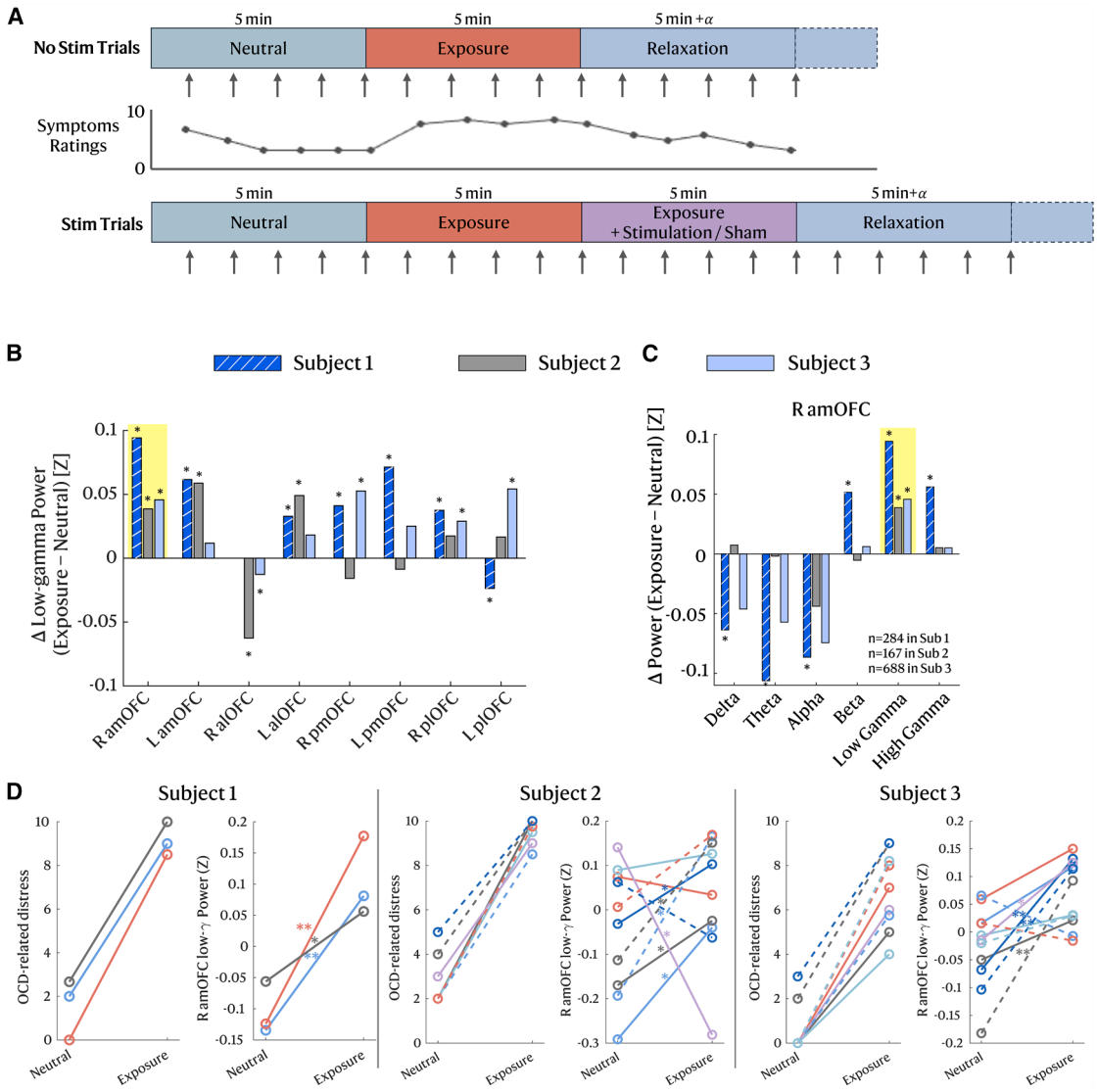

Figure 3. Symptom provocation task paradigm and spectral power changes across frequency bands in OFC subregions

(A) (Top row) A personalized real-world provocation task was designed by a psychologist. The task consisted of 5-min neutral trials and 5-min exposure trials, followed by a relaxation/recovery period (subjects 1, 2, and 3 completed 3, 10, and 11 no-stim trials, respectively). (Middle row) During each trial, behavioral symptom ratings were collected every minute on a tablet. (Bottom row) In Stim Trials, high-frequency right NAc-VeP stimulation was applied during exposure trials to investigate its potential effect on the biomarker and symptom ratings. Each subject underwent a single right NAc-VeP stimulation trial during the Stim Trials phase.

(B) Bar plots show standardized low-gamma power differences between exposure and neutral trials. Exposure to distressing stimuli resulted in significant alterations in low-gamma (30–55 Hz) power across all OFC subregions, with both increases and decreases observed relative to neutral stimuli. Asterisks indicate statistically significant changes (*$p < 0.05$). Recording channels in the right anterior lateral OFC of subject 1 were excluded because of high impedance values during the task.

(C) Notably, all three subjects showed a consistent and significant increase in low-gamma power in the right amOFC during OCD exposure trials compared with the neutral trials (*$p = 1.22e^{-14}$, *$p = 0.014$, and *$p = 9.69e^{-6}$ in subjects 1, 2, and 3, respectively.

(D) Trial-by-trial changes in OCD-related distress and right amOFC low-gamma power during symptom provocation. Each panel shows data from an individual subject, with lines connecting paired neutral and exposure trials. Left column in each subject: OCD-related distress ratings (VAS, 0–10). Right column: low-gamma power (Z scored within channel, averaged across right amOFC contacts). These trial-level line plots highlight the consistency of within-subject changes across trials, complementing the summary statistics in Table S5. Asterisks indicate statistical significance from a trial-level permutation test (*$p < 0.05$, **$p < 0.001$).

See also Figures S2–S4.

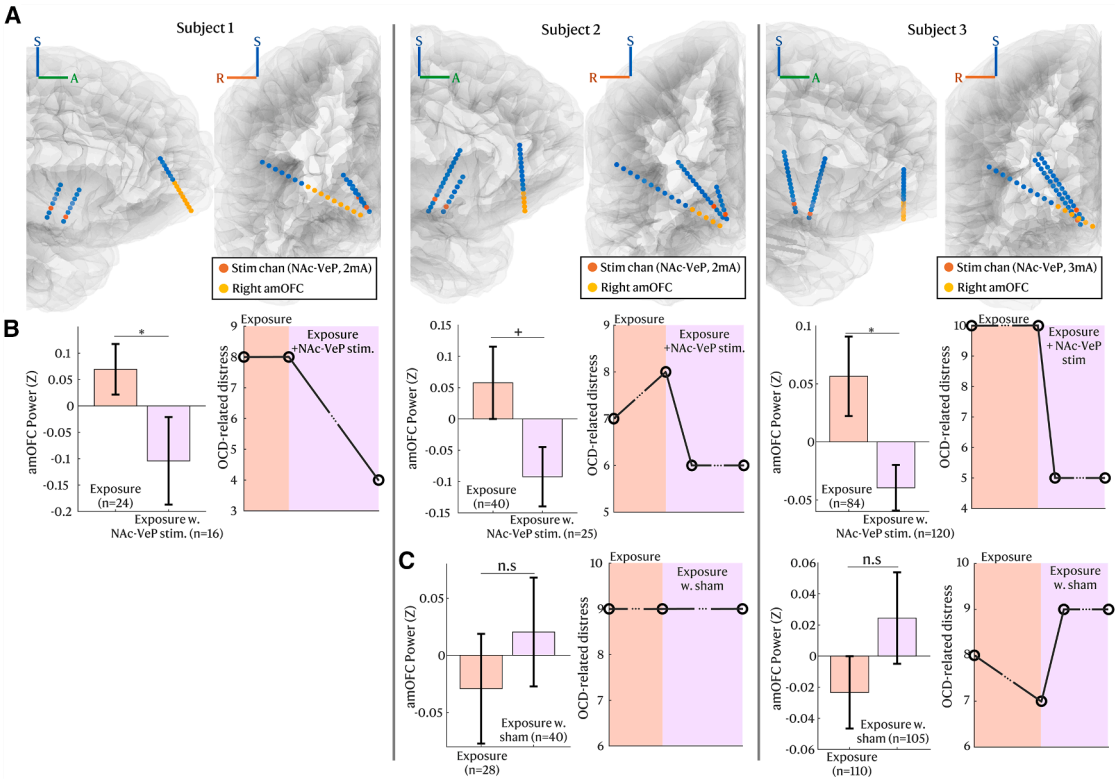

Figure 4. NAc-VeP stimulation reduced amOFC low-gamma power and OCD-related symptoms across three subjects

(A) The top row presents 3D images showing the locations of stimulation channels (Stim channels, orange dots) and the right amOFC (yellow dots) in each subject. (B) The middle row contains two bar plots and a symptom ratings time course graph for each subject. Pink bars represent mean amOFC low-gamma power during OCD exposure without stimulation, while the lavender bars show the same measure during NAc-VeP stimulation. All three subjects exhibited a reduction in amOFC low-gamma power during stimulation (*p = 0.039, ^{+}p = 0.061, *p = 0.008 for subjects 1, 2, and 3, respectively). The plots of symptom severity change show that NAc-VeP stimulation is associated with a reduction in OCD symptom severity across all subjects. Error bars represent standard error of mean (S.E.M.). (C) Sham stimulation during the same task window did not produce a similar reduction in amOFC power (p = 0.4897 in subject 2; p = 0.2186 in subject 3). Results are not available for subject 1, as sham stimulation was not performed in a similar fashion for the first subject. Error bars represent S.E.M.
See also Figure S5.

ensure the results were not driven by global broadband shifts, we also recomputed power changes (Δ in exposure – neutral) after removing the aperiodic component and compared it with the uncorrected power changes (Figure S3). The aperiodic component correction did not alter either the magnitude or direction of the standardized power difference, indicating that the low-gamma band results are not driven by the aperiodic background in this cohort. Also, we did not observe any OFC subregion in which the aperiodic slope (exponent) or offset changed in a statistically significant and same-direction manner across all subjects (Tables S2 and S3).

Pooling all recording sites from all three subjects, the right anterior medial OFC low-gamma band exhibited one of the strongest effects, and this was the only frequency change that was shared across the cohort (β = +0.103, *p = 0.0132). The smallest p across the OFC grid occurred in the left posterior medial OFC in delta (β = −0.156, *p = 0.0002), but this decrease was not consistent across subjects (Figure S2). Other nominal alpha/theta findings did not replicate across all three subjects. Per-cell estimates (Z) and confidence intervals are provided in Table S4, and the effect-size map is shown in Figure S4. All statistics were obtained from a linear mixed-effects model with fixed effects of condition, region, and band and a subject random intercept (see STAR Methods).

Trial-by-trial analysis (Figure 3D; Table S5) showed that 79% of provocation trials across subjects exhibited concordant increases in OCD-related distress and right amOFC low-gamma power (two-sided sign test, *p = 0.0066). Pooled Δpower values were significantly greater than zero (Wilcoxon signed-rank test, *p = 0.0017), indicating consistent co-variation of symptom severity and amOFC low-gamma power at the single-trial level. Thus, amOFC low-gamma power exhibits specificity for dynamic changes in symptom severity, which can potentially be monitored for treatment response.

Targeted NAc-VeP stimulation reduces amOFC gamma power and improves OCD symptom expression during provocation

To validate this biomarker, we examined whether stimulation to the NAc-VeP cluster, the zone exhibiting the most acute therapeutic response (see above), would lead to a reduction in low-gamma power and alleviate OCD symptoms (Figure 4). We

exposed subjects to personalized OCD-provoking triggers for 5 min and subsequently initiated high-frequency NAc-VeP stimulation ipsilateral to the amOFC, where the candidate biomarker was detected, for another 5 min while exposures continued (stim trials in Figure 3A). We compared the magnitude of low-gamma frequency power in the amOFC during the period with and without stimulation. In all three subjects, stimulation led to a decrease in low-gamma frequency power ($^{*}p$ = 0.039, ^{+}p = 0.061, $^{*}p$ = 0.008 in subjects 1, 2, and 3, respectively; Figure 4B), an effect that was not observed during blinded sham stimulation, in which the auditory artifact of stimulation was reproduced but no current was delivered (Figure 4C).

Importantly, the reduction in low-gamma frequency power in the amOFC was associated with a reduction in OCD distress on a VAS rating (see STAR Methods): from 8 to 6, 10 to 5, and 8 to 4 in subjects 1, 2, and 3, respectively (Figure 4B). Improved behavioral patterns were also observed and reported by subjects, e.g., reduced avoidance and ability to engage with previously distressing stimuli. By contrast, during sham stimulation, a decrease in amOFC gamma power was not observed, and there was no improvement in OCD distress on a VAS rating (from 9 to 9 and from 7 to 9 in subjects 2 and 3, respectively) observed (Figure 4C). These findings suggest that the candidate biomarker is functionally tied to fluctuating symptom severity and that its reduction in power reflects a therapeutic response to the acute stimulation.

DISCUSSION

Our study presents evidence that suggests low-gamma power in the amOFC may play a causal role in obsessive-compulsive symptom expression, and effective modulation of this biomarker improves symptom severity. Unlike markers of chronic disease states, this biomarker represents a state-dependent neural signature that fluctuates with moment-to-moment symptom intensity. This distinction is critical in neuropsychiatric conditions, where increasing efforts are made to differentiate markers of illness from dynamic markers of symptom states, as seen in recent findings in depression.[27,28] Our findings suggest that the amOFC may serve as a promising site for state-related biomarker detection in OCD and highlight its potential in future adaptive, closed-loop neuromodulation strategies. Given the heterogeneity of OCD and related behaviors, such network-level biomarker identification represents crucial progress toward personalized therapies.

Our results also underscore the anatomical and functional specificity of the amOFC within the broader prefrontal cortex since other sites did not express the same signal activity.[19,29] The amOFC, which integrates reward valuation and outcome-based behavior,[30] showed consistent biomarker engagement across all three patients. This pattern aligns with our central aim of assessing a conserved/common signal across subjects, i.e., a shared processing mechanism, most clearly expressed as right amOFC low-gamma modulation during provocation. By contrast, other prefrontal regions were not similarly dissociated. This supports existing literature describing distinct cytoarchitectural and connectivity profiles of the medial and lateral OFC,[31,32] highlighting the importance of precise regional mapping when identifying therapeutic targets in OCD.[8]

Building on this, we demonstrated that high-frequency stimulation to ventral structures along the extended ALIC–ventral striatal territory—the NAc-VeP—both alleviated OCD symptoms and reversed the abnormal amOFC gamma activity. This suggests a causal relationship between NAc-VeP stimulation and cortical biomarker modulation. The amOFC strongly projects to the NAc, which itself is interconnected with the adjacent VeP.[33] Outflow of both structures projects back via thalamic routes. Prior work has shown obsession-provoked gamma activity in the NAc,[34] and our findings extend this by demonstrating similar remote cortical activity. The NAc is well-established to be a central node in reward circuitry, and the functionality extends to the VeP in mediating motivational behaviors.[33,35,36] This dual-node stimulation builds upon our prior report of a robust, long-lasting effect of NAc-VeP responsive neurostimulation in a single OCD patient,[23] which corroborates the superior acute, anti-OCD effects observed here compared with stimulation of either node alone.

In addition, our findings add mechanistic support to the frontal-basal ganglia circuit's role in OCD, widely implicated in neuroimaging studies[19,30] but not previously confirmed through direct intracranial electrophysiological and stimulation-based approaches. Importantly, this biomarker modulation we report here occurred during real-time symptom provocation, supporting the feasibility of gamma-based tracking for future adaptive DBS. This aligns with a broader movement toward multi-target network-guided DBS strategies, which may include chronic stimulation of one node, complemented by closed-loop or state-triggered stimulation of another. This dual approach may enhance treatment efficacy, particularly in heterogeneous conditions such as OCD.

Previous studies using electrophysiological recordings at fixed DBS targets have suggested neural signatures of OCD behavioral states in more chronic time scales,[23,34,37,38] though findings across studies have been inconsistent, with no common frequency range signature reported. Notably, in these prior studies, DBS implantation sites were preselected based on convention and intraoperative testing.[39] By contrast, our approach here utilized sEEG to identify individualized biomarker target for targeted modulation. This level of precision may enhance both short- and long-term outcomes in neuromodulatory treatment.

Limitations of the study

We acknowledge several limitations in this study. The sample size is small (n = 3), and stimulation effects were assessed acutely. Because this early feasibility clinical protocol consolidated provocation procedures into brief sessions, each subject underwent only one high-frequency NAc-VeP stimulation trial at a single parameter selected during the target evaluation session. Consequently, within-subject dose or parameter response analyses and trial-by-trial regressions linking low-gamma changes to symptom changes were not feasible. While the observed electrophysiological biomarker in the amOFC was consistent across patients, larger studies will be needed to determine specificity, temporal stability, and suitability for future adaptive stimulation algorithms. Additionally, it remains to be determined if this amOFC biomarker may reflect therapeutic

response over longer timescales. Future work should aim to identify complementary biomarkers—both state-related and trait-level predictors—and test closed-loop DBS strategies in larger, multi-site cohorts to validate generalizability and refine network-informed treatment strategies.

Conclusion

In summary, we provide direct evidence that stimulation of a ventral basal ganglionic target modulates a dynamic biomarker in the amOFC, which is linked to OCD symptoms. These findings offer mechanistic insights into dysregulated network dynamics in OCD and support the development of adaptive, multi-target DBS informed by electrophysiological markers. This work lays the foundation for personalized circuit-based neuromodulation in psychiatric diseases.

RESOURCE AVAILABILITY

Lead contact

Further information and requests for resources and results should be directed to the lead contact, Casey H. Halpern (casey.halpern@pennmedicine.upenn.edu).

Materials availability

This study did not generate new, unique reagents.

Data and code availability

Raw data, including electrophysiology and CT/MRI images newly collected in this study, are not publicly available, as they contain information that could compromise participant privacy or consent, but they will be provided by the lead contact upon reasonable request. This paper does not report original code. Any additional information required to reanalyze the data is available from the lead contact upon request.

ACKNOWLEDGMENTS

This study is funded by the Foundation for OCD Research (FFOR) and AE Foundation. R.L.S. is supported by NINDS T32NS091008 and NIMH R25MH119043 grants. L.Q. is supported by the Brain & Behavior Research Foundation as the Ellen Schapiro & Gerald Axelbaum Investigator. Z.W., J.F.M., and M.S.B. are supported by the National Institutes of Health (5R01MH133717-02). A.H. was supported by the Schilling Foundation, the German Research Foundation (Deutsche Forschungsgemeinschaft, CRC-1451, 431549029), the National Institutes of Health (R01MH130666, 1R01NS127892-01, 2R01MH113929, and UM1NS132358), and the Raynor Cerebellum Project. N.R.W. was primarily supported by grants from the NIH (R01MH122754, UG3NS115637, R01MH128311, and R01MH118388), the Pritzker Neuropsychiatric Disorders Research Consortium (24490), the New Venture Fund (010038-2020-06-01 and 011665-2020-08-01), the Wellcome Trust (220839-1), and funds from Bayshore Global Management. K.W.S. is a consultant for J&J. C.H.H. is supported by the National Institutes of Health (1R01MH124760-01A1, 5UH3NS103446-02, and U01NS117838), the AE Foundation, and the Foundation for OCD Research. The authors would like to thank the study subjects for their participation and commitment to this novel, exploratory application. The authors also acknowledge Dr. Cameron McIntyre for his intellectual contributions during the conceptual development of the project. We dedicate this work to the memory of Dr. Nolan R. Williams, whose insight and contributions were invaluable to this study and many related endeavors.

AUTHOR CONTRIBUTIONS

Y.-H.N.: methodology, investigation, data curation, formal analysis, visualization, and writing – original draft, review, & editing; L.Q.: methodology, investigation, data curation, formal analysis, visualization, and writing – original draft, review, & editing; R.L.S.: methodology, investigation, data curation, project administration, and writing – review & editing; G.C.: investigation and data curation; A.C.: investigation and data curation; Z.W.: data curation, software, and writing – review & editing; J.F.M.: resources, software, and writing – review & editing; M.S.B.: resources, software, and writing – review & editing; D.A.N.B.: conceptualization, investigation, data curation, and writing – review & editing; A H.: methodology, conceptualization, and writing – review & editing; N.R.W.: conceptualization, methodology, supervision, resources, and writing – review & editing; L.A.B.: investigation, data curation, methodology, supervision, and writing – review & editing; T.M.G.: investigation, data curation, and writing – review & editing; M.C.: investigation, data curation, supervision, and writing – review & editing; B.P.: methodology, supervision, resources, and writing – review & editing; D.J.O.: investigation, data curation, supervision, and writing – review & editing; K.J.M.: methodology, formal analysis, supervision, and writing – review & editing; K.W.S.: conceptualization, methodology, supervision, funding acquisition, and writing – review & editing; C.H.H.: conceptualization, methodology, project administration, resources, supervision, funding acquisition, and writing – review & editing.

DECLARATION OF INTERESTS

A.H. reports lecture fees for Boston Scientific, was a consultant for FxNeuromodulation and Abbott in recent years, and serves as a co-inventor on a patent granted to Charité University Medicine Berlin that covers multisymptom DBS fiber filtering and an automated DBS parameter suggestion algorithm unrelated to this work (patent #LU103178). N.R.W. was a named inventor on Stanford-owned intellectual property relating to accelerated TMS pulse pattern sequences, neuroimaging-based TMS targeting, and novel psychedelic intervention for neuropsychiatric disorders; he had served on scientific advisory boards for Otsuka, NeuraWell, Magnus Medical, and Nooma as a paid advisor; he also had equity/stock options in Magnus Medical, NeuraWell, and Nooma. C.H.H. has background patents related to sensing and brain stimulation for the treatment of neuropsychiatric disorders (USPTO serial numbers: 63/170,404 and 63/220,432; international publication number: WO 2022/212891 A1), as well as the use of tractography for circuit-based brain stimulation (USPTO serial number: 63/210,472; international publication number: WO 2022/266000). C.H.H. is a consultant for Boston Scientific, Abbott, Medtronic, and Insightec and receives honoraria for educational lectures. K.W.S. is a consultant for Johnson & Johnson.

STAR★METHODS

Detailed methods are provided in the online version of this paper and include the following:

- KEY RESOURCES TABLE
- EXPERIMENTAL MODEL AND STUDY PARTICIPANT DETAILS
  - Clinical Study
- METHOD DETAILS
  - Image Processing and Electrodes Localization
  - Electrophysiological Data Acquisition
  - Target Evaluation Session
  - Behavioral Symptom Provocation Task
- QUANTIFICATION AND STATISTICL ANALYSIS
  - Electrophysiological Data and Statistical Analysis
  - Linear mixed-effects modeling
- ADDITIONAL RESOURCES

SUPPLEMENTAL INFORMATION

Supplemental information can be found online at https://doi.org/10.1016/j.cell.2025.12.037.

Received: April 18, 2025
Revised: October 1, 2025
Accepted: December 19, 2025
Published: February 5, 2026

REFERENCES

1. Hirschtritt, M.E., Bloch, M.H., and Mathews, C.A. (2017). Obsessive-Compulsive Disorder: Advances in Diagnosis and Treatment. JAMA *317*, 1358–1367. https://doi.org/10.1001/jama.2017.2200.

2. Stein, D.J., Costa, D.L.C., Lochner, C., Miguel, E.C., Reddy, Y.C.J., Shavitt, R.G., van den Heuvel, O.A., and Simpson, H.B. (2019). Obsessive–compulsive disorder. Nat. Rev. Dis. Primers *5*, 52. https://doi.org/10.1038/s41572-019-0102-3.

3. Pallanti, S., Hollander, E., Bienstock, C., Koran, L., Leckman, J., Marazziti, D., Pato, M., Stein, D., and Zohar, J.; International; Treatment; Refractory; OCD Consortium (2002). Treatment non-response in OCD: methodological issues and operational definitions. Int. J. Neuropsychopharmacol. *5*, 181–191. https://doi.org/10.1017/S1461145702002900.

4. Foa, E.B., Yadin, E., and Lichner, T.K. (2012). Exposure and Response (Ritual) Prevention for Obsessive Compulsive Disorder: Therapist Guide (Oxford University Press). https://doi.org/10.1093/med:psych/9780195335286.001.0001.

5. Goodman, W.K., Storch, E.A., and Sheth, S.A. (2021). Harmonizing the Neurobiology and Treatment of Obsessive-Compulsive Disorder. Am. J. Psychiatry *178*, 17–29. https://doi.org/10.1176/appi.ajp.2020.20111601.

6. Milad, M.R., and Rauch, S.L. (2012). Obsessive-compulsive disorder: beyond segregated cortico-striatal pathways. Trends Cogn. Sci. *16*, 43–51. https://doi.org/10.1016/j.tics.2011.11.003.

7. Shephard, E., Stern, E.R., van den Heuvel, O.A., Costa, D.L.C., Batistuzzo, M.C., Godoy, P.B.G., Lopes, A.C., Brunoni, A.R., Hoexter, M.Q., Shavitt, R.G., et al. (2021). Toward a neurocircuit-based taxonomy to guide treatment of obsessive-compulsive disorder. Mol. Psychiatry *26*, 4583–4604. https://doi.org/10.1038/s41380-020-01007-8.

8. Grover, S., Nguyen, J.A., Viswanathan, V., and Reinhart, R.M.G. (2021). High-frequency neuromodulation improves obsessive-compulsive behavior. Nat. Med. *27*, 232–238. https://doi.org/10.1038/s41591-020-01173-w.

9. Horn, A., Li, N., Meyer, G.M., Gadot, R., Provenza, N.R., and Sheth, S.A. (2025). Deep brain stimulation response circuits in obsessive-compulsive disorder. Biol. Psychiatry. S0006-3223(25)01096-0. https://doi.org/10.1016/j.biopsych.2025.03.008.

10. Senova, S., Clair, A.-H., Palfi, S., Yelnik, J., Domenech, P., and Mallet, L. (2019). Deep Brain Stimulation for Refractory Obsessive-Compulsive Disorder: Towards an Individualized Approach. Front. Psychiatry *10*, 905. https://doi.org/10.3389/fpsyt.2019.00905.

11. Gadot, R., Najera, R., Hirani, S., Anand, A., Storch, E., Goodman, W.K., Shofty, B., and Sheth, S.A. (2022). Efficacy of deep brain stimulation for treatment-resistant obsessive-compulsive disorder: systematic review and meta-analysis. J. Neurol. Neurosurg. Psychiatry *93*. jnnp-2021-328738. https://doi.org/10.1136/jnnp-2021-328738.

12. Herrington, T.M., Cheng, J.J., and Eskandar, E.N. (2016). Mechanisms of deep brain stimulation. J. Neurophysiol. *115*, 19–38. https://doi.org/10.1152/jn.00281.2015.

13. Guidetti, M., Marceglia, S., Loh, A., Harmsen, I.E., Meoni, S., Foffani, G., Lozano, A.M., Moro, E., Volkmann, J., and Priori, A. (2021). Clinical perspectives of adaptive deep brain stimulation. Brain Stimul. *14*, 1238–1247. https://doi.org/10.1016/j.brs.2021.07.063.

14. Scangos, K.W., State, M.W., Miller, A.H., Baker, J.T., and Williams, L.M. (2023). New and emerging approaches to treat psychiatric disorders. Nat. Med. *29*, 317–333. https://doi.org/10.1038/s41591-022-02197-0.

15. Ahmari, S.E., and Rauch, S.L. (2022). The prefrontal cortex and OCD. Neuropsychopharmacology *47*, 211–224. https://doi.org/10.1038/s41386-021-01130-2.

16. Rudebeck, P.H., and Murray, E.A. (2014). The Orbitofrontal Oracle: Cortical Mechanisms for the Prediction and Evaluation of Specific Behavioral Outcomes. Neuron *84*, 1143–1156. https://doi.org/10.1016/j.neuron.2014.10.049.

17. Park, H., Kim, M., Kwak, Y.B., Cho, K.I.K., Lee, J., Moon, S.-Y., Lho, S.K., and Kwon, J.S. (2022). Aberrant cortico-striatal white matter connectivity and associated subregional microstructure of the striatum in obsessive-compulsive disorder. Mol. Psychiatry *27*, 3460–3467. https://doi.org/10.1038/s41380-022-01588-6.

18. Beucke, J.C., Sepulcre, J., Talukdar, T., Linnman, C., Zschenderlein, K., Endrass, T., Kaufmann, C., and Kathmann, N. (2013). Abnormally high degree connectivity of the orbitofrontal cortex in obsessive-compulsive disorder. JAMA Psychiatry *70*, 619–629. https://doi.org/10.1001/jamapsychiatry.2013.173.

19. Norman, L.J., Carlisi, C., Lukito, S., Hart, H., Mataix-Cols, D., Radua, J., and Rubia, K. (2016). Structural and Functional Brain Abnormalities in Attention-Deficit/Hyperactivity Disorder and Obsessive-Compulsive Disorder: A Comparative Meta-analysis. JAMA Psychiatry *73*, 815–825. https://doi.org/10.1001/jamapsychiatry.2016.0700.

20. Rauch, S.L., Jenike, M.A., Alpert, N.M., Baer, L., Breiter, H.C., Savage, C.R., and Fischman, A.J. (1994). Regional cerebral blood flow measured during symptom provocation in obsessive-compulsive disorder using oxygen 15-labeled carbon dioxide and positron emission tomography. Arch. Gen. Psychiatry *51*, 62–70. https://doi.org/10.1001/archpsyc.1994.03950010062008.

21. Seilheimer, R.L., Qiu, L., Rocchio, G., Nho, Y.-H., Campos, G., Pesaran, B., Williams, N.R., Rolle, C.E., Buch, V.P., Ganguly, T.M., et al. (2025). Stereo–Encephalography–Guided Multi Lead Deep Brain Stimulation for Treatment–Refractory Obsessive Compulsive Disorder – Study Design and Individualized Surgical Targeting Approach. MedRxiv. https://doi.org/10.1101/2025.04.17.25325961.

22. Mosley, P.E., Windels, F., Morris, J., Coyne, T., Marsh, R., Giorni, A., Mohan, A., Sachdev, P., O'Leary, E., Boschen, M., et al. (2021). A randomised, double-blind, sham-controlled trial of deep brain stimulation of the bed nucleus of the stria terminalis for treatment-resistant obsessive-compulsive disorder. Transl. Psychiatry *11*, 190. https://doi.org/10.1038/s41398-021-01307-9.

23. Nho, Y.-H., Rolle, C.E., Topalovic, U., Shivacharan, R.S., Cunningham, T.N., Hiller, S., Batista, D., Feng, A., Espil, F.M., Kratter, I.H., et al. (2023). Responsive deep brain stimulation guided by ventral striatal electrophysiology of obsession durably ameliorates compulsion. Neuron *112*, 73. 83.e4. S0896-6273(23)00747-X. https://doi.org/10.1016/j.neuron.2023.09.034.

24. Nuttin, B., Cosyns, P., Demeulemeester, H., Gybels, J., and Meyerson, B. (1999). Electrical stimulation in anterior limbs of internal capsules in patients with obsessive-compulsive disorder. Lancet *354*, 1526. https://doi.org/10.1016/S0140-6736(99)02376-4.

25. Mar-Barrutia, L., Ibarrondo, O., Mar, J., Real, E., Segalàs, C., Bertolín, S., Aparicio, M.A., Plans, G., Menchón, J.M., and Alonso, P. (2022). Long-term comparative effectiveness of deep brain stimulation in severe obsessive-compulsive disorder. Brain Stimul. *15*, 1128–1138. https://doi.org/10.1016/j.brs.2022.07.050.

26. Hamlett, G.E., Foa, E.B., and Brown, L.A. (2023). Exposure Therapy and Its Mechanisms. In Fear Extinction: From Basic Neuroscience to Clinical Implications, M.R. Milad and S.D. Norrholm, eds. (Springer International Publishing), pp. 273–288. https://doi.org/10.1007/7854_2023_428.

27. Scangos, K.W., Khambhati, A.N., Daly, P.M., Makhoul, G.S., Sugrue, L.P., Zamanian, H., Liu, T.X., Rao, V.R., Sellers, K.K., Dawes, H.E., et al. (2021). Closed-loop neuromodulation in an individual with treatment-resistant depression. Nat. Med. *27*, 1696–1700. https://doi.org/10.1038/s41591-021-01480-w.

28. Scangos, K.W., Makhoul, G.S., Sugrue, L.P., Chang, E.F., and Krystal, A.D. (2021). State-dependent responses to intracranial brain stimulation in a patient with depression. Nat. Med. *27*, 229–231. https://doi.org/10.1038/s41591-020-01175-8.

29. Provenza, N.R., Rajesh, S.V., Reyes, G., Katlowitz, K.A., Pugalenthi, L.S., Bechtold, R.A., Diab, N., Reddy, S., Allam, A.K., Gandhi, A.D., et al. (2025). High beta power in the ventrolateral prefrontal cortex indexes human

approach behavior: a case study. J. Neurosci. *45*, e1321242025. https://doi.org/10.1523/JNEUROSCI.1321-24.2025.

30. Wood, J., and Ahmari, S.E. (2015). A Framework for Understanding the Emerging Role of Corticolimbic-Ventral Striatal Networks in OCD-Associated Repetitive Behaviors. Front. Syst. Neurosci. *9*, 171. https://doi.org/10.3389/fnsys.2015.00171.
31. Henssen, A., Zilles, K., Palomero-Gallagher, N., Schleicher, A., Mohlberg, H., Gerboga, F., Eickhoff, S.B., Bludau, S., and Amunts, K. (2016). Cytoarchitecture and probability maps of the human medial orbitofrontal cortex. Cortex *75*, 87–112. https://doi.org/10.1016/j.cortex.2015.11.006.
32. Kahnt, T., Chang, L.J., Park, S.Q., Heinzle, J., and Haynes, J.-D. (2012). Connectivity-Based Parcellation of the Human Orbitofrontal Cortex. J. Neurosci. *32*, 6240–6250. https://doi.org/10.1523/JNEUROSCI.0257-12.2012.
33. Haber, S.N., and Knutson, B. (2010). The reward circuit: linking primate anatomy and human imaging. Neuropsychopharmacology *35*, 4–26. https://doi.org/10.1038/npp.2009.129.
34. Miller, K.J., Prieto, T., Williams, N.R., and Halpern, C.H. (2019). Case Studies in Neuroscience: The electrophysiology of a human obsession in nucleus accumbens. J. Neurophysiol. *121*, 2336–2340. https://doi.org/10.1152/jn.00096.2019.
35. Ottenheimer, D., Richard, J.M., and Janak, P.H. (2018). Ventral pallidum encodes relative reward value earlier and more robustly than nucleus accumbens. Nat. Commun. *9*, 4350. https://doi.org/10.1038/s41467-018-06849-z.
36. Richard, J.M., Ambroggi, F., Janak, P.H., and Fields, H.L. (2016). Ventral Pallidum Neurons Encode Incentive Value and Promote Cue-Elicited Instrumental Actions. Neuron *90*, 1165–1173. https://doi.org/10.1016/j.neuron.2016.04.037.
37. Provenza, N.R., Sheth, S.A., Dastin-van Rijn, E.M., Mathura, R.K., Ding, Y., Vogt, G.S., Avendano-Ortega, M., Ramakrishnan, N., Peled, N., Gelin, L.F.F., et al. (2021). Long-term ecological assessment of intracranial electrophysiology synchronized to behavioral markers in obsessive-compulsive disorder. Nat. Med. *27*, 2154–2164. https://doi.org/10.1038/s41591-021-01550-z.
38. Vissani, M., Nanda, P., Bush, A., Neudorfer, C., Dougherty, D., and Richardson, R.M. (2022). Toward Closed-Loop Intracranial Neurostimulation in Obsessive-Compulsive Disorder. Biol. Psychiatry *93*, e43–e46. https://doi.org/10.1016/J.BIOPSYCH.2022.07.003.
39. Shofty, B., Gadot, R., Viswanathan, A., Provenza, N.R., Storch, E.A., McKay, S.A., Meyers, M.S., Hertz, A.G., Avendano-Ortega, M., Goodman, W.K., et al. (2022). Intraoperative valence testing to adjudicate between ventral capsule/ventral striatum and bed nucleus of the stria terminalis target selection in deep brain stimulation for obsessive-compulsive disorder. J. Neurosurg. *139*, 442–450. https://doi.org/10.3171/2022.10.JNS221683.
40. Wang, Z., Magnotti, J.F., Zhang, X., and Beauchamp, M.S. (2023). YAEL: Your Advanced Electrode Localizer. eNeuro *10*. ENEURO.0328-23.2023. https://doi.org/10.1523/ENEURO.0328-23.2023.
41. Magnotti, J.F., Wang, Z., and Beauchamp, M.S. (2020). RAVE: Comprehensive open-source software for reproducible analysis and visualization of intracranial EEG data. NeuroImage *223*, 117341. https://doi.org/10.1016/j.neuroimage.2020.117341.
42. Fischl, B. (2012). FreeSurfer. NeuroImage *62*, 774–781. https://doi.org/10.1016/j.neuroimage.2012.01.021.
43. Avants, B.B., Tustison, N.J., Song, G., Cook, P.A., Klein, A., and Gee, J.C. (2011). A reproducible evaluation of ANTs similarity metric performance in brain image registration. NeuroImage *54*, 2033–2044. https://doi.org/10.1016/j.neuroimage.2010.09.025.
44. Schalk, G., McFarland, D.J., Hinterberger, T., Birbaumer, N., and Wolpaw, J.R. (2004). BCI2000: A General-Purpose Brain-Computer Interface (BCI) System. IEEE Trans. Biomed. Eng. *51*, 1034–1043. https://doi.org/10.1109/TBME.2004.827072.

STAR★METHODS

KEY RESOURCES TABLE

REAGENT or RESOURCE	SOURCE	IDENTIFIER
Software and algorithms		
MATLAB R2024a	The MathWorks	https://www.mathworks.com/
FieldTrip 2021.10.20	FieldTrip toolbox	https://www.fieldtriptoolbox.org/
RAVE: Reproducible Analysis & Visualization of iEEG	BeauchampLab	https://rave.wiki/
BCI2000	National Center for Adaptive Neurotechnologies	https://www.bci2000.org/
FreeSurfer	Laboratory for Computational Neuroimaging	https://surfer.nmr.mgh.harvard.edu
ANTs (Advanced Normalization Tools)	Penn image computing and science laboratory	https://stnava.github.io/ANTs/
Other		
sEEG electrodes	Ad-Tech	https://adtechmedical.com/
EEG system / stimulator	g.tec	https://www.gtec.at/

EXPERIMENTAL MODEL AND STUDY PARTICIPANT DETAILS

Clinical Study

Three subjects were enrolled in an ongoing clinical trial (NCT05623306; IDE# G220185) of stereo-encephalography (sEEG) guided multi-target deep brain stimulation (DBS) for treatment-resistant obsessive-compulsive disorder (trOCD).[21] This trial afforded our team the opportunity here to further the understanding of the network hypothesis of OCD. Data for this current investigation is obtained in the first stage of the clinical study, where subjects undergo sEEG-based brain mapping in the psychiatric monitoring unit, while psychologist-led symptoms provocations are conducted under direct clinical observation.

Major inclusion criteria for the study include age 25–75 years old (inclusive), meeting Diagnostic and Statistical Manual of Mental Disorders, Fifth Edition guidelines (DSM-5) diagnostic criteria of chronic (>5 years) OCD; severe OCD as defined by Y-BOCS score of $\geq$28 and a lack of adequate response after adequate treatment trials, including $\geq$2 selective serotonin reuptake inhibitors, clomipramine, $\geq$1 augmentation trial with an antipsychotic medication and adequate trials of cognitive-behavior therapy based exposure and response prevention. Major exclusion criteria included any other primary psychiatric diagnosis defined in the DSM-5, including Hoarding disorder, secondary diagnosis of bipolar I or II disorder, anorexia nervosa, bulimia nervosa or binge eating disorder, or psychotic or mood disorder with psychotic features as defied in DSM-5; current suicidal risk defined by the Columbia Suicide Severity Rating Scale; Dependency, addiction or abuse or overuse of illicit substances including alcohol; History of head trauma with loss of consciousness for > 5 minutes or residual effect unresolved by a year, abnormal neuroimaging study or more than 1 head injury within past two years diagnosed as concussion, concussive-type or traumatic brain injury; Any permanent cardiac, brain implant or implanted medical pumps.

All three subjects fulfilled eligibility criteria and were enrolled in the study. Subject 1 was a 38-year-old male diagnosed with OCD since age 11. His baseline Y-BOCS score was 40 and his primary symptom included pathological doubt and intrusive thoughts. Subject 2 was a 62-year-old female who was diagnosed with OCD from age 16. Her baseline Y-BOCS score was 38 and primary symptoms include contamination, cleaning compulsions, difficulty with thought processes and distorted sensory perceptions. Subject 3 was a 26-year-old female diagnosed with OCD 8 years prior, with symptoms starting around age 9. Her baseline Y-BOCS score was 44 and primary symptoms include contamination.

METHOD DETAILS

Image Processing and Electrodes Localization

High-resolution magnetic resonance imaging (MRI) sequences (T1, T2-weighted and Fast Gray Matter Acquisition T1 Inversion Recovery [FGATIR]) were obtained for all subjects. Following sEEG electrodes implantation for each subject, a high-resolution, full-tissue-range computer tomography (CT) of the head was acquired and co-registered to pre-operative MRI using YAEL module of Reproducible Analysis and Visualization of iEEG software (RAVE).[40,41] Three-dimensional coordinates of each sEEG electrode contact were computed with RAVE. Atlas-based image segmentation using FreeSurfer[42] as well as two-step linear and non-linear co-registration using Advanced Normalization Tools (ANTs)[43] with affine and asymmetric normalization were implemented within the RAVE pipeline. Each sEEG electrode was assigned an anatomical label based on the segmentation and verified independently by

two investigators (L.Q. and G.C.) Electrode contacts located in the amOFC, pmOFC, alOFC, plOFC, and structures within the extended ventral striatal territory were identified for subsequent electrophysiological analyses.

Electrophysiological Data Acquisition

Subjects underwent sEEG implantation with up to sixteen custom Ad-Tech sEEG electrodes (SD08R-AP58X-000, SD16R-AP02X-000, SD16R-AP03X-000, RD16R-SP03X-000) (up to total 240 electrode contacts) placed bilaterally spanning various cortical and subcortical brain anatomical targets that have been reported to be involved in trOCD. These sEEG targets and trajectories were determined based on a multi-disciplinary team consensus comprising neurosurgeons, neuroanatomists and psychiatrists, and included the orbitofrontal cortices (anterior and posterior), frontal pole, ventrolateral prefrontal cortices, anterior cingulate cortices, anterior limb of the internal capsule, nucleus accumbens, ventral pallidum, subthalamic nucleus, dorsolateral hippocampus and basolateral amygdala. All sEEG probes had a DBS-like configuration with 1.1 mm diameter with 8–16 electrode contacts of 1.32 mm length and 2–3 mm center-to-center distance. (Ad-Tech, Oak Creek, WI.) Once stereo-EEG electrode leads were implanted, they were connected via four headboxes to a 256-channel g.HIamp system (amplifier; g.tec, Schiedlberg, Austria) for continuous neural signal recording at a sampling rate of 1200Hz. A switching unit connects the g.Estim PRO system (stimulator) to allow concurrent stimulation and recording without the need for manual switching. The BCI2000 software is used to integrate multimodal recording and analysis to allow integration across data capture devices (continuous video recordings, audiovisual presentation hardware) and synchronized timestamping to behavioral data.[44]

Target Evaluation Session

A comprehensive safety assessment was performed under the supervision of an epileptologist to explore safety limits of stimulation across all contact pairs. Bipolar stimulation was performed across each pair of contacts in 0.5mA increment from 0 to 6mA, 60–90μs, 100–130Hz. Once stimulation thresholds were established, systematic target evaluation was performed with 1 minute- and 5-minute-long stimulation testing over five days. Subjects' subjective rating of OCD-related distress were recorded on a visual analog scale (VAS) of 0–10 before and after each stimulation. Subjects were blinded to the stimulation target and condition. Stimulation parameters that elicited positive or negative effects were noted. Repeated evaluation of potential targets were conducted over subsequent of the study in the psychiatric monitoring unit. To minimize perceptual differences between stimulation and sham, subjects were told that audible noise would occur during both conditions. Subjects were instructed to focus on their immediate behavioral state rather than on guessing the stimulation condition, but were encouraged to report in real-time any unusual sensations or changes in behavioral or emotional state. No formal reporting about perceived stimulation versus sham was performed. However, these active and sham stimulation trials were performed after initial safety screening, where any contacts that induced side effects were eliminated from further testing. Thus, subjects were not expected to be able to identify the stimulation condition.

In this investigation, we delivered acute DBS to components of the extended ALIC–ventral striatal territory, including the NAc, VeP, and ALIC—the FDA-approved target for OCD under humanitarian device exemption (Figure S1). We also tested stimulation of the NAc-VeP complex, previously reported to produce rapid and sustained symptom improvement.[23] To quantify the effectiveness of each stimulation site, we calculated percentage reduction in symptoms and effect size (Cohen's *d*) in Figures 2C and 2D; Table S1. 1) The percentage reduction was determined by comparing the average symptom severity before and after stimulation. Specifically, the difference between the pre-stimulation and post-stimulation scores was divided by the pre-stimulation score and expressed as a percentage. This metric provides a relative measure of symptom improvement for each condition. 2) To quantify the effect size, we used Cohen's *d*, which measures the magnitude of symptom change relative to variability. The effect size was calculated by dividing the difference between the mean pre-stimulation and post-stimulation symptom scores by the pooled standard deviation of both conditions. A larger Cohen's *d* indicates a stronger effect of stimulation on symptom reduction. These measures allowed for a standardized comparison of the therapeutic effects of different stimulation targets during the Target Evaluation Session ($d \approx 0.2$ = small, > 0.5 = medium, > 0.8 = large effect).

Behavioral Symptom Provocation Task

Prior to sEEG implantation, a full interview is conducted by a trained psychologist with each subject to understand their OCD-related symptoms and relevant provocations. The psychologist, in collaboration with the study team, designed a set of real-world provocation trials, consisting of 5-minute-long neutral trials and 5-minute-long exposure trials, followed by a relaxation/recovery period (Figure 3A). The duration of the relaxation/recovery period varied based on the subject's condition. During the task, behavioral symptom ratings (OCD-related distress) were obtained on a tablet every minute using a 0 to 10 VAS, where 0 represents no symptoms and 10 represents the most severe symptoms. The onset of the task was recorded in the BCI2000 software to synchronize this event with the intracranial EEG (iEEG) data. Throughout the task, continuous audiovisual and iEEG recordings were obtained.

The behavioral symptom provocation task was performed on eight out of the 12 days of hospitalization (Days 3–5 and 7–11). During the first three consecutive days (Days 3–5), trials were conducted without stimulation (No Stim Trials, Figure 3A). In the remaining days (Days 7–11, Stim Trials, Figure 3A), stimulation was applied to targets selected based on the Target Evaluation Session. No Stim Trials were used to identify the biomarker shown in Figures 3B, 3C, and S2. Then, Stim Trials were used to investigate the potential modulation of the biomarker. Subjects were blinded to the stimulation target and condition. Each subject underwent a right NAc-VeP stimulation trial during Stim Trials phase. The stimulation parameters had been determined in the Target Evaluation Session

that best reduced distress. Given the limited time available during hospitalization, it was not feasible to conduct Stim Trials across all evaluated targets. Therefore, we prioritized stimulation at the NAc-VeP target, which exhibited the most robust initial clinical response and had previously demonstrated therapeutic efficacy in our prior work.[23] The stimulation parameters in Subjects 1 and 2 were 2mA in amplitude, 130Hz frequency, and 90μs pulse width at NAc(+)-VeP(-) in a bipolar configuration. Unfortunately, data collection during the exposure trial with right NAc-VeP stimulation alone for Subject 3 could not be completed due to a software freeze caused by the stimulator's battery depletion. However, we successfully recorded a trial with a combination stimulation paradigm which included the right NAc(+)-VeP(-) (3mA, 130Hz, 90μs) and the right rostral anterior cingulate cortex (ACC; 3mA, 130Hz, 90μs) stimulation simultaneously using two stimulators. Notably, isolated stimulation of the right rostral ACC increased the OCD-distress on a VAS rating from 4 to 8 and did not modulate the low-gamma power in amOFC (p=0.9917) during the behavioral symptom provocation task (Figure S5), which suggested positive effects in this trial were predominantly due to NAc-VeP stimulation.

QUANTIFICATION AND STATISTICL ANALYSIS

Electrophysiological Data and Statistical Analysis

All synchronized behavioral, audiovisual, and electrophysiological data were exported to MATLAB for offline analysis. A 1-minute data window preceding each symptom rating was extracted based on synchronized timestamps. The raw iEEG data were processed using a bandpass filter from 1 to 120 Hz and a notch filter at 60 and 120 Hz with a 4 Hz bandwidth. The filtered data were then segmented into 5-second, non-overlapping windows, and each contact was bipolar-referenced to the adjacent contact on the same electrode. The frequency bands analyzed in this study are defined as follows: delta (1–4Hz), theta (5–8Hz), alpha (9–12Hz), beta (13–30Hz), low-gamma (30–55Hz), and high-gamma (65–115Hz).

Bad channels and epochs were rejected based on a combination of recorded channel impedance values and visual inspection to ensure clean data. Spectral power was extracted using multi-taper fast Fourier transform with a Hanning taper from 1 to 115 Hz (1:1:115 Hz). For each session, the spectral power of each channel was standardized using Z-scoring. The standardized spectral power for each channel was then averaged across No Stim Trials. To obtain the spectral power in the OFC subregions (left and right, anterior and posterior, and medial and lateral OFC; Figures 3B, 3C, and S2), spectral power was averaged across all recorded channels in the same OFC subregion, excluding those identified as white matter contacts based on anatomical imaging.

The spectral power difference during NAc-VeP stimulation was calculated by comparing exposure conditions with and without stimulation, using a within-subject design in each subject. In this session, the spectral power of each channel was standardized using Z-scoring and then averaged across all recorded channels in the right amOFC (Figures 4B and 4C). A permutation test (n=1000 permutations) was used to assess differences in spectral power between neutral vs. exposure trials (Figures 3B, 3C, and S2) and exposure trials with vs. without stimulation (Figures 4B and 4C). For each comparison, spectral power values were randomly shuffled across conditions to generate a null distribution of mean differences. The observed mean difference was then compared against this distribution to compute an empirical two-tailed p-value.

Linear mixed-effects modeling

Trial-level power was Z-scored within channel. We fit a linear mixed-effects model, power $\sim$ condition $\times$ region $\times$ band + (1|subject), with fixed effects of condition (neutral vs exposure), region (8 OFC subregions), and frequency band (delta, theta, alpha, beta, low gamma, high gamma), and subject as random intercept (Figure S4). Fixed-effect inference used marginal F tests with residual degrees of freedom. For each region $\times$ band cell, the exposure vs neutral simple effect was obtained from the same model by re-leveling that cell to the reference; we report estimate (β), two-sided p values, and 95 percent confidence intervals. Full per-cell statistics and multiplicity summaries (within-band families of 8 regions per band) are provided in Table S4.

ADDITIONAL RESOURCES

Clinical Trial Registration: Stereo-Encephalography–Guided Multi-Target Deep Brain Stimulation for Treatment-Resistant Obsessive-Compulsive Disorder

ClinicalTrials.gov Identifier: NCT05623306

CellPress
OPEN ACCESS

Supplemental figures

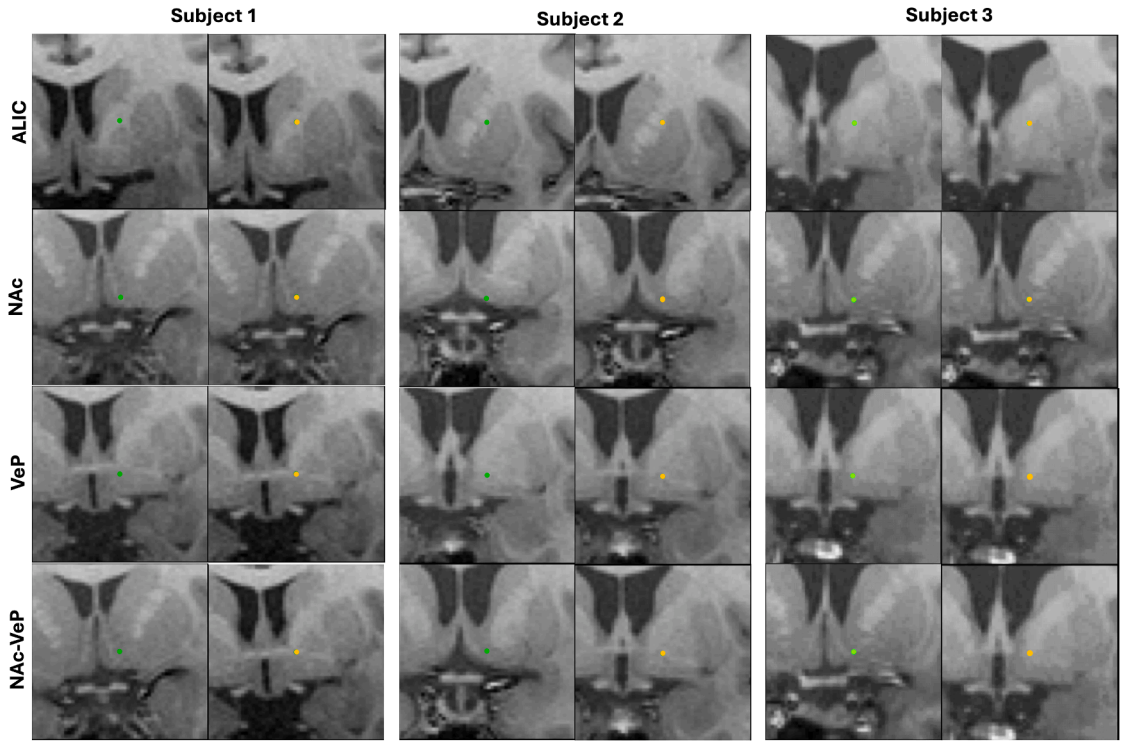

Figure S1. Locations of subcortical stimulation electrode contacts, related to Figure 1

Coronal MRI images of bipolar stimulation contact pairs for each subject and stimulation sites in ALIC (top row), NAc (second row), VeP (third row), and NAc-VeP (bottom row). For each subject, the left column is the anode (+, green), and the right column is the cathode (−, yellow). Locations of subcortical stimulation electrode contacts, related to Figure 1.

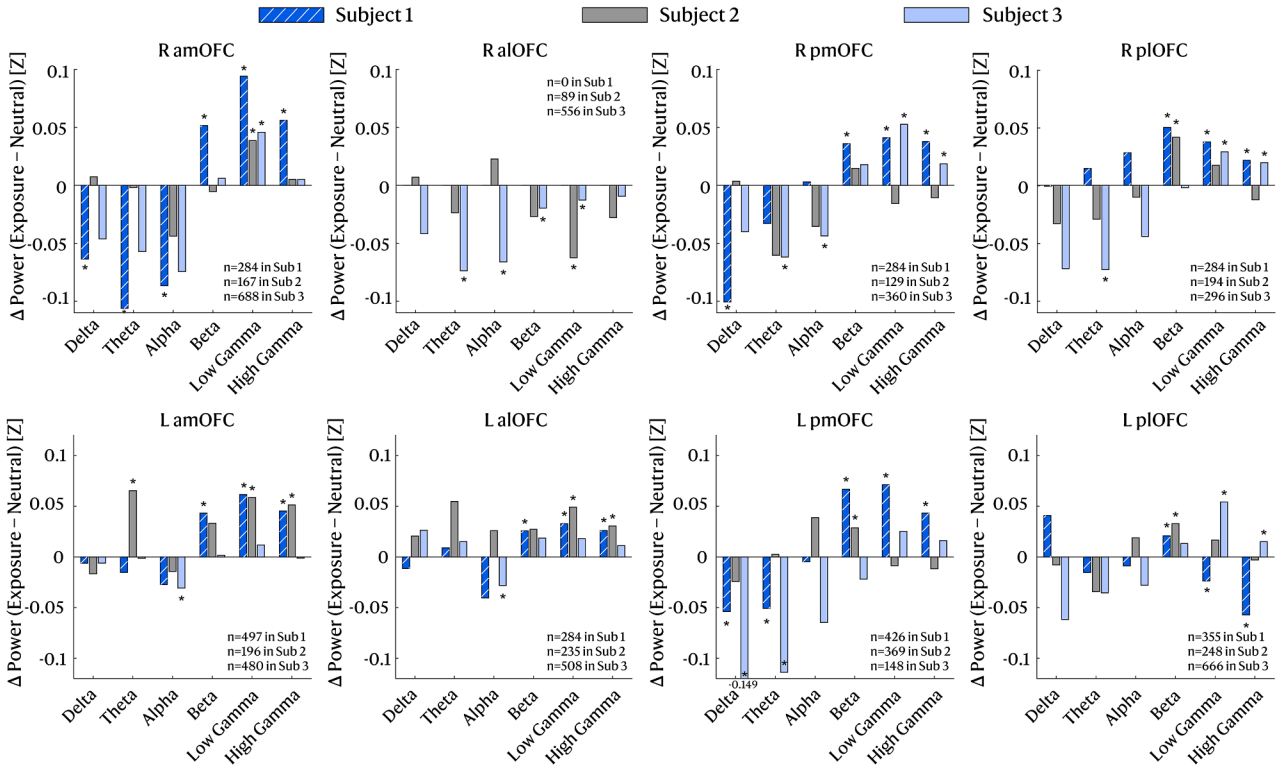

Figure S2. Standardized power (Z) differences between exposure and neutral trials across six frequency bands for each subject in the OFC subregions, related to Figure 3

Asterisks indicate statistically significant changes (*$p < 0.05$). Notably, all three subjects showed a consistent and significant increase in low-gamma power in the right amOFC during OCD exposure trials compared with the neutral trials (*$p = 1.22e^{-14}$, *$p = 0.014$, *$p = 9.69e^{-6}$ in subjects 1, 2, and 3, respectively). Recording channels in the right anterior lateral OFC of subject 1 were excluded because of high impedance values during the task.

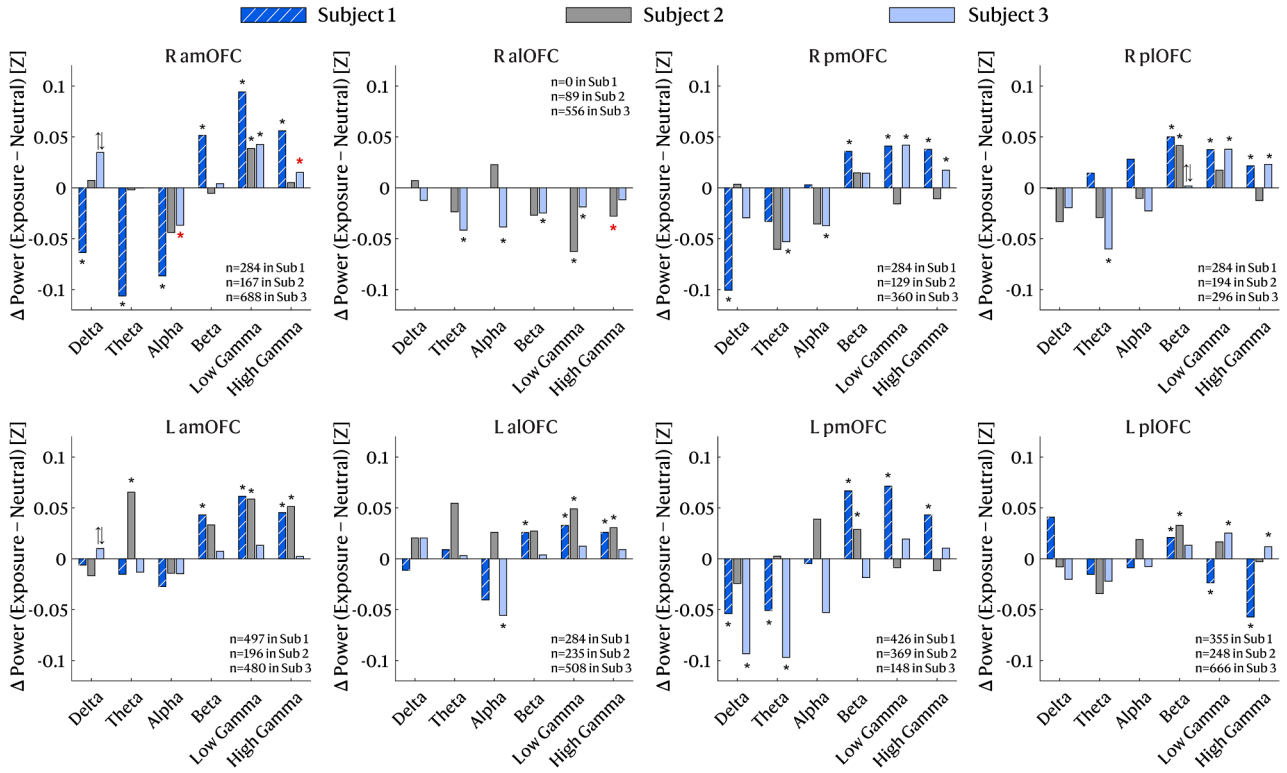

Figure S3. Standardized power (Z) differences between exposure and neutral trials across six frequency bands for each subject in the OFC subregions, after correction for the aperiodic component, related to Figure 3

Asterisks indicate statistically significant changes (*$p < 0.05$), whereas red asterisks mark conditions that newly reached significance after aperiodic correction. Opposite-direction symbols (↑↓) denote sign reversals relative to the uncorrected results (Figure S2), none of which were statistically significant. Overall, aperiodic correction did not substantially alter either the magnitude or direction of the standardized power (Z) differences, indicating that the observed low-gamma band results are not driven by the aperiodic background.

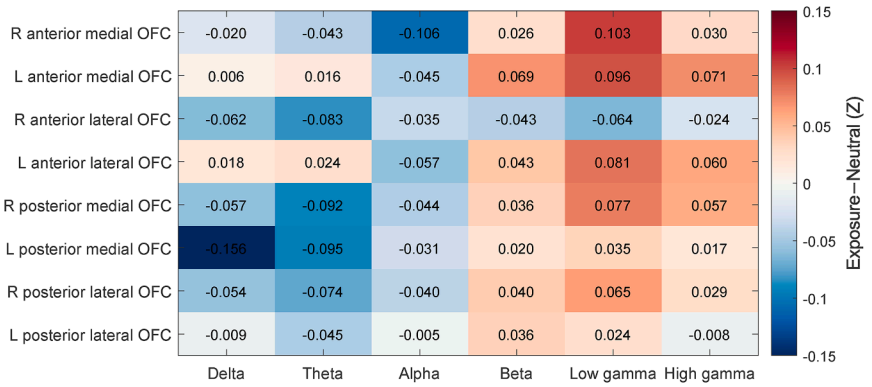

Figure S4. Heatmap of hierarchical linear mixed-effects model simple-effect estimates (β) of provocation-related power change (exposure – neutral, Z units) for each region and frequency band, related to Figure 3

Rows represent OFC subregions (R/L anterior medial, anterior lateral, posterior medial, and posterior lateral), and columns represent frequency bands. Color scale represents hierarchical linear mixed-effects model fixed-effect estimates for the exposure–neutral contrast. The largest effects are seen in low-gamma power within the amOFC bilaterally.

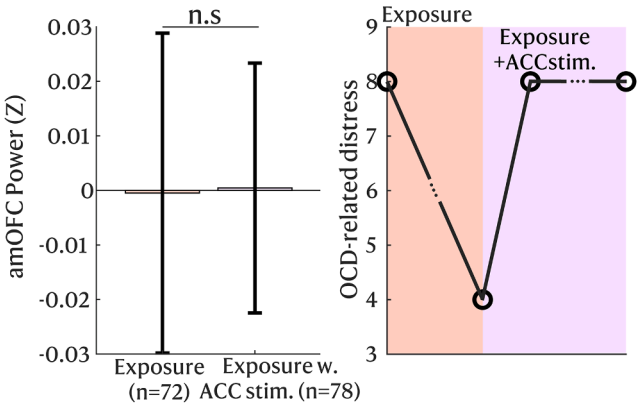

Figure S5. Effects of isolated right rostral ACC stim on right amOFC low-gamma frequency band power and OCD-related distress in subject 3, related to Figure 4

Data collection during the exposure trial with right NAc-VeP stimulation alone for subject 3 could not be completed due to a software freeze caused by the stimulator's battery depletion. However, a trial with simultaneous dual-site stimulation (right NAc-VeP and right rostral ACC) was recorded and shown. Notably, single-site stimulation of the right rostral ACC alone increased the OCD-related distress on a VAS rating from 4 to 8 and did not modulate the low-gamma power in amOFC during the symptom provocation task (p = 0.9917).